












Interband Short Reach Data Transmission in Ultrawide Bandwidth Hollow Core Fiber

H. Sakr , Member, OSA, Y. Hong , Member, IEEE, T. D. Bradley , Member, IEEE, Member, OSA, G. T. Jasion , Member, OSA, J. R. Hayes , Member, IEEE, Member, OSA, H. Kim , I. A. Davidson, E. Numkam Fokoua, Y. Chen, Member, IEEE, K. R. H. Bottrill , N. Taengnoi , N. V. Wheeler, Member, IEEE, P. Petropoulos , Fellow, OSA, D. J. Richardson , Fellow, IEEE, and F. Poletti , Senior Member, IEEE

(Post-Deadline Paper)

Abstract—We report a Nested Antiresonant Nodeless hollow-core Fiber (NANF) operating in the first antiresonant passband. The fiber has an ultrawide operational bandwidth of 700 nm, spanning the 1240–1940 nm wavelength range that includes the O-, S-, C- and L- telecoms bands. It has a minimum loss of 6.6 dB/km at 1550 nm, a loss ≤ 7 dB/km between 1465–1655 nm and ≤ 10 dB/km between 1297–1860 nm. By splicing together two structurally matched fibers and by adding single mode fiber (SMF) pigtailed at both ends we have produced a ~ 1 km long span. The concatenated and connectorized fiber has an insertion loss of approximately 10 dB all the way from 1300 nm to 1550 nm, and an effectively single mode behavior across the whole spectral range. To test its data transmission performance, we demonstrate 50-Gb/s OOK data transmission across the O-to L-bands without the need for optical amplification, with bit-error-rates (BERs) lower than the 7% forward error correction (FEC) limit. With the help of optical amplification, 100-Gb/s PAM4 transmission with BER lower than the KP4 FEC limit was also achieved in the O/E and C/L bands, with relatively uniform performance for all wavelengths. Our results confirm the excellent modal purity of the fabricated fiber across a broad spectral range, and highlight its potential for wideband, low nonlinearity, low latency data transmission.

Index Terms—Fiber optics communications, hollow core optical fibers, microstructured optical fibers.

Manuscript received June 24, 2019; revised September 5, 2019 and September 16, 2019; accepted September 19, 2019. Date of publication September 23, 2019; date of current version December 30, 2019. This work was supported in part by the European Research Council project LightPipe (682724), in part by the Engineering and Physical Sciences Research Council, U.K., under Grant EP/P030181/1, and in part by the Royal Academy of Engineering. (Corresponding author: Francesco Poletti.)

H. Sakr, Y. Hong, T. D. Bradley, G. T. Jasion, J. R. Hayes, I. A. Davidson, E. N. Fokoua, Y. Chen, K. R. H. Bottrill, N. Taengnoi, N. V. Wheeler, P. Petropoulos, D. J. Richardson, and F. Poletti are with the Optoelectronics Research Centre, University of Southampton, Southampton SO17 1BJ, U.K. (e-mail: h.sakr@soton.ac.uk; y.hong@soton.ac.uk; t.bradley@soton.ac.uk; g.jasion@soton.ac.uk; jrhh@orc.soton.ac.uk; i.a.k.Davidson@soton.ac.uk; eric.numkam-fokoua@soton.ac.uk; yc1m12@soton.ac.uk; k.bottrill@soton.ac.uk; nt1a15@soton.ac.uk; nww1v10@orc.soton.ac.uk; pp@orc.soton.ac.uk; djr@orc.soton.ac.uk; frap@orc.soton.ac.uk).

H. Kim is with the Optoelectronics Research Centre, University of Southampton, Southampton SO17 1BJ, U.K., and also with the Electrical and Electronic Convergence Department, Hongik University, Sejong 30016, South Korea (e-mail: h.kim@soton.ac.uk).

Color versions of one or more of the figures in this article are available online at <http://ieeexplore.ieee.org>.

Digital Object Identifier 10.1109/JLT.2019.2943178

I. INTRODUCTION

HOLLOW core fibers (HCF) offer lower latency and nonlinearity than conventional fibers [1]. Major advances have been made in HCF technology in recent years, to the point that state-of-the-art (SoTA) fibers now show performance levels that are compatible with a variety of short reach data transmission applications. The first generation of HCFs (produced ~ 15 years ago) were photonic bandgap fibers (PBGFs), in which the termination of the periodic cladding to create the core-guiding defect resulted in the formation of surface modes. This narrowed the fibers' usable bandwidth to 10s of nanometers, and although the loss in these fibers was very low (~ 1 – 2 dB/km) [2], reliable data transmission was impractical [3]. A second generation of PBGFs, free from surface modes (in the operating window), offered bandwidths of ~ 100 nm, losses of a few dB/km [4], and were shown to be capable of supporting high capacity data transmission [5].

More recently, the air-guiding bandwidth was increased to several 100 s of nanometers through the introduction of nodeless hollow core antiresonant fibers (ARFs). These offered octave-spanning bandwidth, albeit at the expense of a higher loss [6], [7]. A 7 capillary 'tubular' ARF with a '3 dB' bandwidth (i.e., bandwidth at which the dB/km loss doubles from its minimum value) of 700 nm (950–1650 nm) and a minimum loss of 25 dB/km was reported. Penalty-free data transmission at 1, 1.5 and 2 μm was demonstrated in a single fiber, although only at 10 Gbit/s and over just 100 m [8]. An even lower loss was achieved in the same fiber type by optimizing the dimensions of the tubes [7], however this work did not include fibers designed to operate at telecoms wavelengths.

The next major evolutionary step was to add additional azimuthally oriented membranes to improve leakage loss. This can be done by either adding thin glass membranes inside each capillary [9] or, as demonstrated in this work, by adding 'nested' capillaries inside each antiresonant tube. Such nested antiresonant nodeless fibers (NANFs) promise—in theory—optical losses lower than those of standard silica fibers [10]. The first reported low-loss NANF was designed to operate in the *second* antiresonant passband (which we will refer to as the *second* passband) to reduce the fabrication challenges. This allowed the

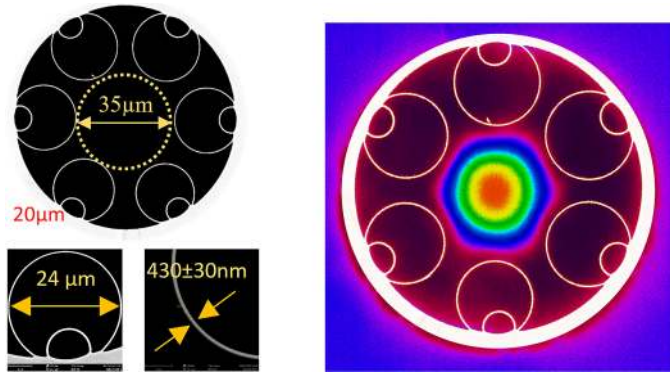


Fig. 1. (a) SEM images of the fabricated NANF for this work and details of the microstructured cladding including core OD, average outer tubes diameter and thickness. The inter-tube azimuthal gaps are between $6.1 \mu\text{m}$ to $7.7 \mu\text{m}$; (b) measured mode field image when light was launched into the fiber with a broadband supercontinuum source.

use of relatively thick ($\sim 1 \mu\text{m}$) tube membranes, which can be produced using only moderate preform inflation during the fiber draw and hence reasonably wide process tolerances. Using this approach, a single mode, *second* passband NANF with a record minimum loss for any data transmitting HCF of 1.3 dB/km was reported [11]. Its ‘3 dB’ bandwidth of 128 nm was sufficient to accommodate C- and L-band transmission, but not wide enough to cover other telecoms windows/bands.

In this work, we report a NANF operating in the *first* antiresonant passband (which we will refer to as *first* passband; Fig. 1), which requires thinner struts than *second* passband NANFs and is consequently more difficult to fabricate. Its minimum loss of 6.6 dB/km at 1550 nm is the lowest reported amongst any ARF operating in the *first* antiresonant passband. Structural asymmetries and some relatively large inter tube gaps mean that the loss is higher than that of ref. [11]. However, the fiber offers a 3dB bandwidth of 700 nm ($1240\text{--}1940 \text{ nm}$), well in excess of the O+E+S+C+L-band range. To demonstrate its potential for data transmission across different telecoms windows and over km distance scales, we spliced this fiber to a similar structurally matched fiber, and connectorized the whole assembly. The excellent modal properties of these HCFs allowed us to achieve penalty-free 50 Gbit/s OOK and 100 Gbit/s PAM4 data transmission over $\sim 1 \text{ km}$ of fiber in the $1291\text{--}1631 \text{ nm}$ spectral range. It is believed that NANFs offer a very promising solution for future high-speed, low-latency intra/inter datacenter, 5G and short-reach optical communications especially for mobile fronthaul applications.

II. FABRICATION AND CHARACTERIZATION

The fiber was produced using a stack, fuse and draw process, and is composed of 6 nested tubes defining a hollow core with a diameter of $35 \pm 0.5 \mu\text{m}$ as shown in Fig. 1. Initially, 6 nested capillary elements were stacked and fused inside a jacket tube. The assembly was then drawn into canes, which were then jacketed and drawn down to fiber dimensions (in a second draw stage). Control of the fiber microstructure, including the core, inner and outer tube expansion ratio, was achieved via a specialized pressurization system and was supported by in-line

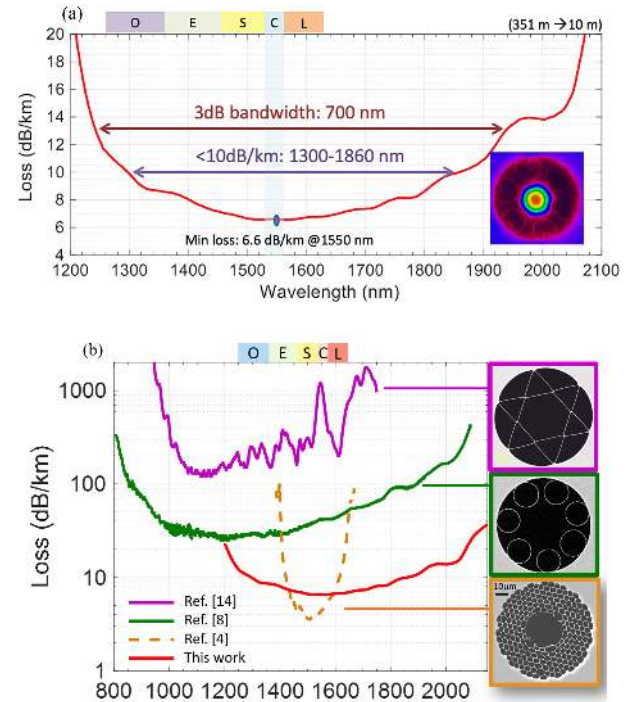


Fig. 2. (a) Measured loss spectrum of the reported NANF; (b) loss of the fabricated NANF (red curve) compared to previous generations of ultrawide bandwidth antiresonant fibers operating in the 2nd and 3rd telecoms window (purple: ‘hexagram ARF with nodes’ [14], and green: nodeless tubular ARF [8]); a SoTA wide bandwidth data-transmitting PBGF is also shown for comparison (orange, dashed [4]).

fluid dynamics modelling [12]. The outer tubes of the NANF elements shown in Fig. 1 have outer diameters (OD) ranging from $22.2 \mu\text{m}$ to $25.2 \mu\text{m}$ and strut thicknesses (t) ranging from 405 nm to 462 nm (average $430 \pm 30 \text{ nm}$). The nested inner tubes have ODs ranging from $8.9 \mu\text{m}$ to $10 \mu\text{m}$ and strut thicknesses ranging from 457 nm to 514 nm (average $480 \pm 30 \text{ nm}$). The inter-tube azimuthal gaps are between $6.1 \mu\text{m}$ to $7.7 \mu\text{m}$, and these values are maintained throughout the full fiber length.

The optical loss of this fiber was measured over the full fiber bandwidth using the cutback method. This was performed using a tungsten lamp white light source (WLS) and two optical spectrum analyzers (a Yokogawa AQ-6315A covering the $400\text{--}1750 \text{ nm}$ wavelength range, and a Yokogawa AQ-6375A covering the $1200\text{--}2400 \text{ nm}$ wavelength range). A 2-nm resolution was used over the full fiber bandwidth. A 351 m length of the fiber was spooled on a 1-m circumference bobbin and this was cut back to 10 m . Three separate spectral transmission traces from three different output cleaves were recorded for both the long and the short lengths without perturbing the launch conditions, and these were averaged to ensure reliable measurements. Fig. 2(a) presents the measured cutback loss of the fabricated NANF, showing a minimum loss of 6.6 dB/km at 1550 nm , a loss $\leq 7 \text{ dB/km}$ from 1465 nm to 1655 nm and $\leq 10 \text{ dB/km}$ between $1297\text{--}1860 \text{ nm}$ [13]. To the best of our knowledge, this is the lowest loss ever reported for an ultrawide bandwidth HCF operating in the *first* passband. The measured loss is compared in Fig. 2(b) to that of previous generations of ultrawide bandwidth HCFs operating around telecoms wavelengths: a hexagram ARF fiber

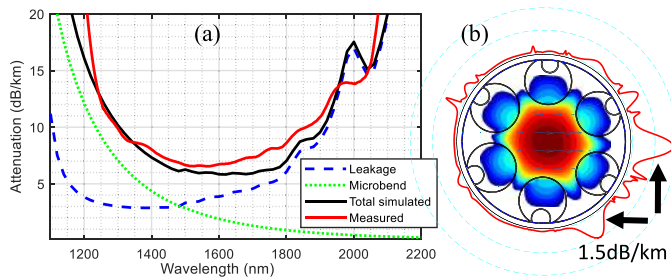


Fig. 3. (a) Measured (solid red) vs. simulated loss of the NANF reported herein; (b) simulated fundamental mode and its radial Poynting vector at 1550 nm, showing that a considerable fraction of the loss arises from the gaps created by one smaller than the average tube.

with nodes (~ 150 dB/km) [14] and the tubular fiber mentioned in the introduction (~ 25 dB/km) [8]. For reference, the loss of a SoTA wide bandwidth PBGF (3.5 dB/km) [4] for which several C-band DWDM transmission experiments have been reported is also shown. Comparing these previous wide bandwidth HCFs, the tradeoff between loss and bandwidth/flatness can be readily appreciated.

Despite its already good optical properties, some structural non-uniformities, such as non-ideal inter-tube gaps or slightly misaligned inner capillaries are present in the fabricated fiber. These non-uniformities have a strong influence on the total measured loss and to a lesser extent the bandwidth of operation. To further understand where the loss arises in the fabricated fiber and to analyze the effect of the small structural non-uniformities that can be seen in Fig. 1 on its optical behavior, we extracted its cross-section from an SEM image and simulated its performance using the modelling tools described in ref. [11]. The theoretically calculated loss includes: (a) surface scattering contributions (*cf.* ref. [10]); (b) confinement loss using FEM calculations; and (c) microbend loss contributions (*cf.* ref. [15]). As can be seen in Fig. 3(a), overall, the total simulated loss (black line) is in good agreement with the measurement (red line). It is also clear that leakage loss dominates at longer wavelengths i.e., >1700 nm, whilst the main contribution at shorter wavelengths 1100–1450 nm can be attributed to microbending. Generally, for the structure reported in this work, the contribution of surface scattering loss (SSL) is very small and according to simulations is <0.07 dB/km at 1550 nm. This is due to the fact that all membranes in NANF operate in antiresonance and are therefore effective at keeping the density electromagnetic field low at the glass-air interfaces. The most dominant contributions to the total loss are leakage loss (dotted blue) and microbending loss (dotted green). On the other hand, from Fig. 3(a), the peak around $2 \mu\text{m}$ in the simulated curve could be attributed to structural resonance, i.e., anticrossings with modes in the glass tubes [10]. Given the high aspect ratio between length and thickness of the glass tubes, the overlap between air and glass modes are small but still sufficient to create the oscillations observed in the loss plot [16]. For the measured curve, a small but noticeable peak at $\sim 1.95 \mu\text{m}$ followed by a dip at $2 \mu\text{m}$ could be observed, which could be attributed to the same phenomena. Additionally and/or

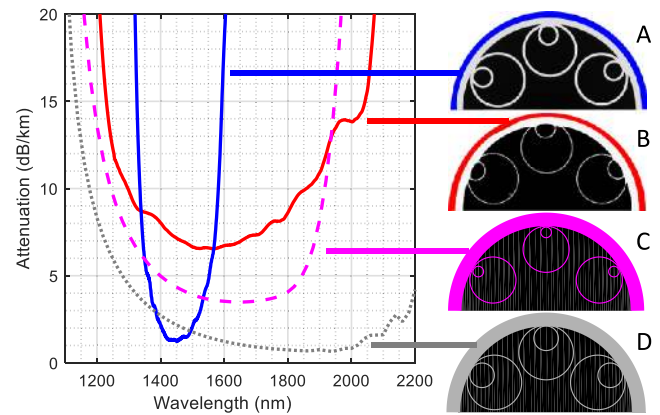


Fig. 4. Measured Loss of the NANF reported in ref. [11] (A; solid blue) vs. current fiber (B; *cf.* Fig. 1; solid red). Also shown is the simulated optical loss of an ideal geometry, allowing for regular inter-tube gaps with the same average size as in the fabricated fiber (C; gaps of $6.5 \mu\text{m}$; dashed purple), and with small inter-tube gap size (D; gaps of $2 \mu\text{m}$; dotted grey).

alternatively, an roto-vibrational overtone from CO_2 is also present at $\sim 1.96 \mu\text{m}$, which might give rise to some absorption.

Fig. 3(b) shows the simulated longitudinal Poynting vector of the fundamental mode of the fiber at 1550 nm wavelength, as well as the intensity of its radial component at the outer boundary of the fiber (red line around the microstructure). It can be seen that considerable leakage (a total of ~ 1.5 dB/km, or $\sim 1/3$ of the total leakage loss at 1550 nm) occurs through two gaps at either side of one of the tubes, which has a diameter that is $\sim 2 \mu\text{m}$ smaller than the others. This smaller than average tube is likely to originate from minor imperfections in the starting cane used to draw the final fiber and can certainly be addressed as the fabrication technology evolves. In this case we attribute the cause of the smaller tube to a slightly misplaced inner capillary (see bottommost tube in Fig. 1(b)) which has led to local thickening of the glass layer which in turn has led to reduced expansion under pressure compared to the other tubes.

Fig. 4 shows a comparison between the loss of the NANF reported here (see Fig. 1) designed to operate in the *first* passband, and that reported in ref. [11] with a minimum loss of 1.3 dB/km and fabricated to operate in the *second* passband. Although operating in the *first* passband offers the advantage of greater operational bandwidth, more than double that of a fiber operating in the *second* passband, the control over the fiber's structure during fabrication is much more challenging. Simulations indicate that reducing the azimuthal inter-tube gap is crucial to reduce the leakage loss contribution in NANFs [11]. However, achieving small gaps has proven to be experimentally difficult for fibers fabricated to operate in the *first* passband. This can be attributed to the thinner tube membranes (which are almost half the thickness of those in *second* passband fibers) and that makes them considerably more sensitive to subtle changes in the applied pressure and to the initial size of the tubes within the preform or cane. As a result of this, the azimuthal inter-tube gaps in the fabricated fiber were of the order of $\sim 6.5 \mu\text{m}$ on average, two to three times as large as those already achieved

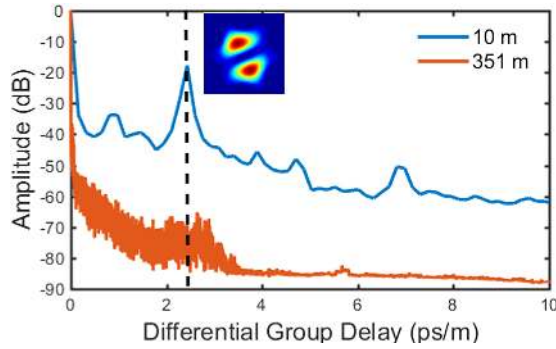


Fig. 5. S^2 measurement of the reported NANF showing that no appreciable high order mode content remains after 350 m.

in the 1.3 dB/km NANF in ref. [11], or in the 2.5 dB/km NANF that operates at 1100 nm in ref. [17]. To reach better understanding of the effect of the structural imperfections in the fabricated fiber, we also simulated the optical loss of an ideal NANF with no structural asymmetries, allowing for regular gaps with the same average size as in the fabricated fiber ($6.5 \mu\text{m}$), and with the same average size ($2 \mu\text{m}$) as the *second* passband fiber in ref. [11]. Drawing the same fiber without asymmetries would lead to the dashed loss curve in Fig. 4, with a minimum loss of 3.5 dB/km. Additionally, reducing the gap size to only $2 \mu\text{m}$, which we believe should be ultimately achievable with further improvements in fabrication control, would produce a sub 1-dB/km fiber (dotted curve in Fig. 4).

It is worth mentioning that although producing NANFs in the *second* passband could be relatively easier than in the *first* passband in terms of fabrication precision and control over the structure, it is believed that achieving similar structures with low loss and small inter-tube gaps to that in ref. [11] could be achieved in the very near future in NANFs produced in the *first* passband. In general, in order to improve on the uniformity of the fiber structure which results in a more controlled azimuthal inter-tube gaps it is important to control the uniformity of the structure in the canes to start with. This could be improved by the initial design, stacking and manufacturing of the canes. Additionally in order to improve on the azimuthal inter-tube gaps in the fibers, better control and precision over the applied pressure in the fibre draw is necessary. None of these issues is fundamental in origin, and further progress is expected in the very near future. Additionally, drawing NANFs in the *first* passband offers multiple advantages such as a flatter ultrawide transmission bandwidth that could be >3 times that of a *second* passband fiber; and an almost doubling of the yield.

Furthermore, in HC-ARFs the higher order modes (HOMs) are always fundamentally lossier than the fundamental mode, LP_{01} ; this is further enhanced when utilizing the NANF structure, due to its intrinsic mode-stripping geometry that couples core guided high order modes to modes in the cladding tubes [10]. As a result of this, the fabricated NANF was found to be effectively single mode after a length of 350 m, as confirmed by an S^2 cutback measurement. As can be seen in Fig. 5, an LP_{11} mode contribution could still be observed after only 10 m

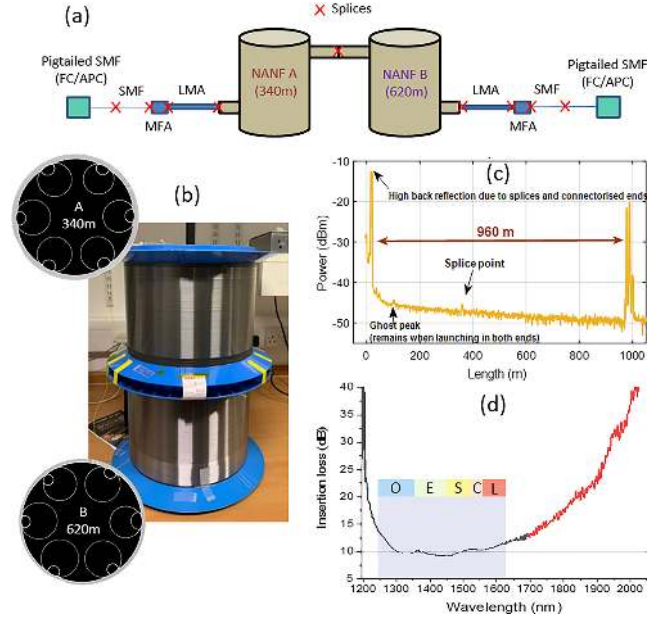


Fig. 6. (a) Schematic of the fully spliced 960-m span comprising of two structurally matched lengths of NANF; (b) SEM images and photograph of the spliced fiber; (c) OTDR trace of the span measured at $\lambda = 1550 \text{ nm}$ highlighting reflection from the spliced joint; (d) insertion loss of the spliced span which shows $10.15 \pm 0.15 \text{ dB}$ at 1300 nm and $10.26 \pm 0.15 \text{ dB}$ at 1550 nm.

of propagation, with an intensity of 17 dB below that of the fundamental mode. As a result of the large differential loss, the LP_{11} mode is heavily suppressed relative to the LP_{01} mode and hence disappears in the noise floor after 350 m, with a relative intensity of $\sim -75 \text{ dB}$. Moreover, simulations of the ideal geometries shown in Fig. 4(c) and 4(d) and predict that the relative HOM extinction could reach 300x for fabricated inter-tube gaps of $6.5 \mu\text{m}$, and up to 1000x for smaller gaps of $2 \mu\text{m}$.

III. WIDE-BAND DATA TRANSMISSION EXPERIMENT

A. $\sim 1 \text{ km}$ Band Span Preparation

Following the production and characterization of the 351 m long NANF reported above (341 m after the cutback measurement; NANF A in Fig. 6), a second, structurally matched and 620 m long fiber (NANF B in Fig. 6), was fabricated. Both NANFs were spliced together to form a single $\sim 1 \text{ km}$ span for data transmission tests, as shown in Fig. 6(a). The two NANFs were spliced together using a commercial splicer, Fujikura FSM 100P. The splicer parameter were controlled to optimize the splice in terms of transmission and to try to preserve the microstructure. The fibers were cladding-aligned. The rotational (θ axis) mismatch did not give any noticeable change on splicing loss. Weak arc power was used to give minimum damage to the microstructure. Moreover, the $\sim 1 \text{ km}$ span was fully-connectorized with relatively low splicing losses. Initially, both HCFs were spliced to each other with a measured splice loss of $\sim 0.1 \text{ dB}$ (NANF A to NANF B; SEM images are shown in Fig. 6(b)). This band was then spliced at both ends to SMF using a combination of intermediate mode field diameter (MFD)

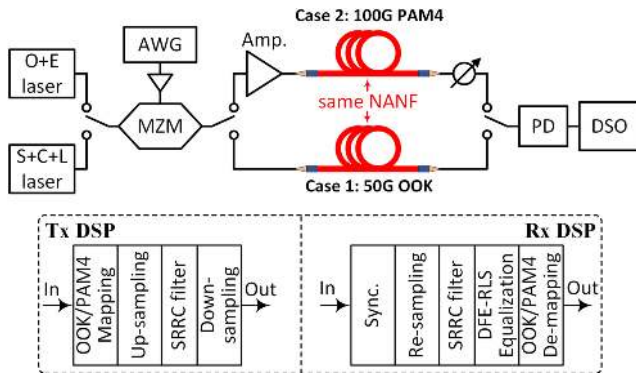


Fig. 7. Setup of the transmission experiment using the NANF and the offline DSP blocks.

matching solid fibers including mode mode field adaptors (MFA) and single large mode area fibers (LMA). From 1300 to 1600 nm the mode field diameter of the hollow core fiber does not change significantly; it does however vary quite substantially in the MFD matching fibers. We therefore decided to exploit this fact to equalise the spectral loss of the overall ~ 1 km band. We did so by optimizing the MFD of the bridging fiber so that it produced a minimum loss at a wavelength of 1300 nm where the fiber loss was higher. This produced a higher splicing loss at 1550 nm, which increases the overall insertion loss at these wavelengths and explains the flatter overall spectral loss profile shown in Fig. 6(d) as compared to that of NANF A (in Fig. 2(a)). Further, to validate the full length of the spliced fiber, and to check for longitudinal defects, the fiber span was examined using OTDR at $\lambda = 1550$ nm which also detected the spliced point at the anticipated relevant length, and is presented in Fig. 6(c).

B. Setup of the Transmission Experiment

To evaluate the wideband data-transmission capability of the spliced fiber, we conducted high-speed Nyquist on-off keying (OOK) and 4-ary pulse-amplitude modulation (PAM4) data transmission experiments in different telecom bands (O- to L-band). The setup of the transmission experiment and the corresponding digital signal processing (DSP) diagram is shown in Fig. 7. At the transmitter end, two tunable lasers, covering the 1291–1372 nm (O+E band) and 1461–1631 nm (S+C+L band) wavelength ranges, were used as a continuous-wave (CW) source to be modulated using a Mach-Zehnder LiNbO₃ modulator (MZM). The offline-generated Nyquist-OOK/PAM4 signals were fed into an arbitrary waveform generator (AWG, Keysight M8196A) for digital-to-analogue conversion at a fixed sampling rate of 90 GSa/s. The output of the AWG was first amplified by an electrical amplifier and then used to modulate the MZM. As shown in Fig. 7, two different cases were considered in the experiments: in Case 1, the MZM was modulated by 50-Gb/s OOK signals and its output was directly launched into the NANF without any optical amplification. The output of the tunable laser was fixed at 7 dBm for wavelengths shorter than 1600 nm whilst a 2-dB increment was applied to longer wavelengths mainly to compensate for the increased insertion loss of the MZM.

At the receiver, after the photodiode (PD, Finisar XPRV2022A), the detected signals (10^5 symbols) were recorded by a digital storage oscilloscope (DSO) with a sampling rate of 80 GSa/s. In Case 2, either a bismuth- or an erbium-doped fiber amplifier was used to amplify the MZM's output for the O/E and C/L bands, respectively, before launching the signal into the NANF. 100-Gb/s PAM4 signals were adopted in this case for data transmission, since a higher optical signal-to-noise ratio was available. After the NANF, an optical attenuator was used to attenuate the optical power incident to the PD. In both cases, as shown in Fig. 7, no polarization control was adopted at the input of the NANF, as the NANF has a low polarization dependent loss (PDL) [18]. It is worth mentioning that similar to [19], the low PDL ensures the feasibility of polarization division multiplexed coherent transmission using the fabricated NANF. However, commercially available coherent receivers will currently limit the transmission in the NANF to around the C-band despite the fact that other bands might also be usable for transmission.

In the offline DSP, the mapped OOK/PAM4 symbols were first up-sampled and then filtered by a square-root raised cosine (SRRC) filter with a roll-off factor of 0.1. Subsequently, down-sampling was applied to generate either 50-Gb/s OOK or 100-Gb/s PAM4 signals. At the receiver end, the captured signals were synchronized and re-sampled before being filtered by a matching SRRC filter. After that, a half-symbol-spaced (17, 7)-tap decision-feedback equalizer (DFE) with the recursive least squares (RLS) algorithm was applied for signal recovery. The forgetting factor of the RLS algorithm was 0.99. Finally, the reconstructed OOK/PAM4 signals were de-mapped for bit-error-rate (BER) calculation via error counting.

C. Transmission Results

Fig. 8 shows the results of the 50-Gb/s OOK transmission (Case 1) across the O- to L-band. The received optical powers (ROPs) of the tested wavelengths were around -15 dBm. The resulting signal-to-noise ratios (SNRs) were around 11.5 dB. Thanks to the relatively uniform ROP/SNR performance, the corresponding BERs in all bands were lower than the 7% forward error correction (FEC) limit, i.e., 3.8×10^{-3} , therefore no optical amplification was required. Note that the performance degradations at wavelengths shorter than 1300 nm and around 1600 nm are principally attributed to the higher insertion loss of the MZM at these wavelengths. Since an E-band tunable laser was not available, only two wavelengths in the E-band, i.e., 1361 nm and 1371 nm, were investigated in both cases. For reference, the remaining untested wavelength range is highlighted in Fig. 8. Nevertheless, comparable BER/ROP/SNR performance can be expected since the fiber attenuation is similar to that of the neighboring bands, as shown in the characterization in Section III.A. For reference, the eye diagrams of the signals transmitted at the wavelengths of 1331 nm and 1551 nm are also provided in Fig. 8. The corresponding BERs are 2.33×10^{-4} and 2.0×10^{-4} , respectively.

The results of Case 2 (100-Gb/s PAM4 transmission) are shown in Fig. 9. These demonstrate that comparable ROP/SNR

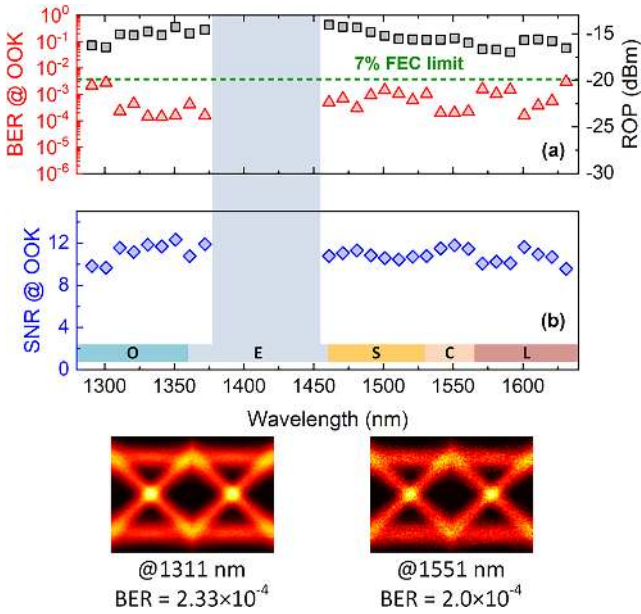


Fig. 8. (a) BER and ROP versus wavelengths for 50-Gb/s OOK transmission and (b) the corresponding SNR versus wavelengths. Insets: eye diagrams of the 1311-nm and 1551-nm wavelengths.

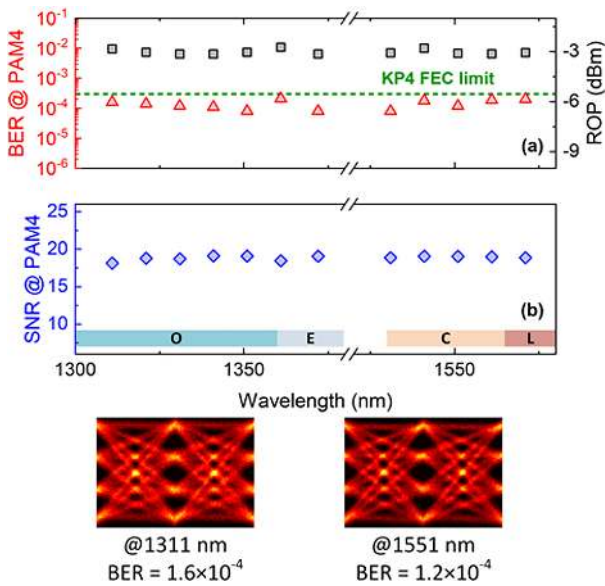


Fig. 9. (a) BER and ROP versus wavelengths for 100-Gb/s PAM4 transmission and (b) the corresponding SNR versus wavelengths. Insets: eye diagrams of the 1311-nm and 1551-nm wavelengths.

performance can be achieved across the investigated wavelengths in the O, E, C and L bands. The ROP and SNR levels of the tested wavelengths were around -3 dBm and 18.5 dB, respectively, and the corresponding BERs of all wavelengths are below the KP4 FEC limit (3×10^{-4}) [20]. We note that since lower BERs were obtained for the 100-Gb/s PAM4 transmission, the KP4 FEC limit is assumed in Fig. 9, as the KP4-FEC requires shorter overhead (approximately 3%) and its induced latency is also much lower [21].

For reference, the eye diagrams of the recovered PAM4 signals at 1311 nm and 1551 nm are presented in Fig. 9 as well, and

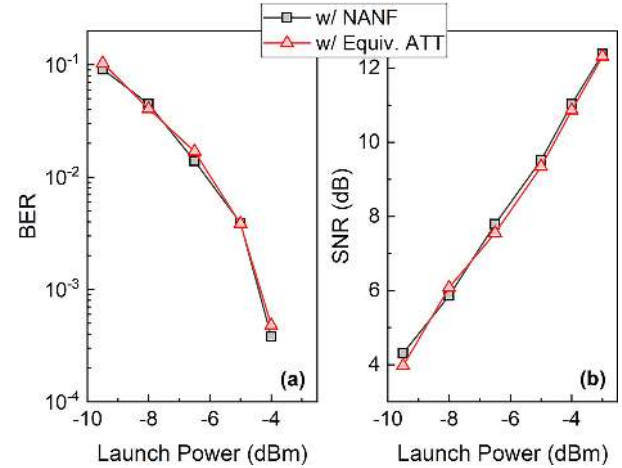


Fig. 10. Performance comparison with back-to-back for the 1550-nm channel with 50-Gb/s OOK: (a) BER and (b) SNR.

their BERs are 1.6×10^{-4} and 1.2×10^{-4} , respectively. It is also worth noting that the tunable lasers and optical amplifiers in Case 2 were not fully driven, that is, their output powers were kept relatively low. Considering the ultra-low nonlinearity of the hollow-core fibers [19], much higher launch powers could be tolerated for data transmission. Therefore, much higher capacities per wavelength and/or much longer transmission distances should be easily achievable. Furthermore, since the optical beams within the NANF are air-guided, the chromatic dispersion (CD) effect of the bands of interest in the NANF is negligible. It is also worth noting that when further extending the reach to beyond just a few kilometres, it is anticipated that the NANF will not suffer from the severe power fading thanks to its low CD. In contrast, for a standard single-mode fibre, the CD-induced power fading will limit the performance of the OOK/PAM4 transmission. Therefore, a significant improvement in the transmission performance is expected by using the NANF technology. This point will be further investigated in a following study.

We further compared the performance between the scenarios of NANF transmission and back-to-back transmission (wherein an optical attenuator with an equivalent loss was adopted). The comparisons of the 50-Gb/s OOK and the 100-Gb/s PAM4 cases at 1550 nm are shown in Fig. 10 and Fig. 11, respectively. For both cases, nearly identical BER and SNR performance to that of the back-to-back scenario was achieved when using the NANF, indicating that no additional penalty arose from the transmission in the NANF. This results from the effective single-mode guiding properties of the NANF which ensures that any penalty induced by coupling to higher-order modes is negligible.

It is worth noting that although most of the recently reported HCF transmission experiments including this work are demonstrated in short-reach optical interconnects, long-reach transmission using HCF can be expected upon the realisation of long-length and low-loss HCFs. With further refined fabrication process, longer yields of HCFs can be realistically fabricated. With regard to propagation loss, the loss of the NANF can be significantly reduced to sub-dB/km level over

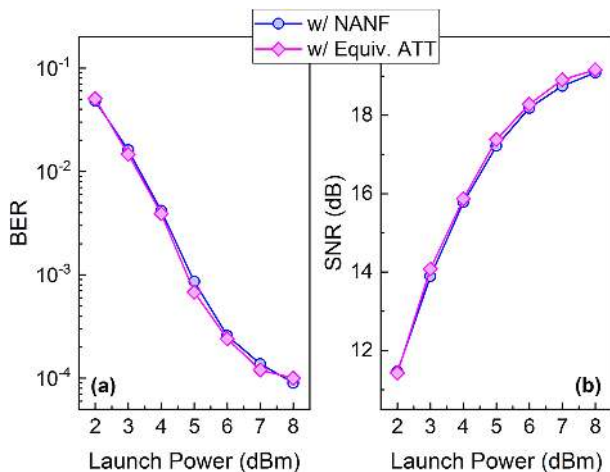


Fig. 11. Performance comparison with back-to-back for the 1550-nm channel with 100-Gb/s PAM4: (a) BER and (b) SNR.

an ultrawide spectrum range when using the optimised fibre design and refined fabrication control, as discussed in Section II. Furthermore, in principle, NANFs can achieve lower losses than standard silica fibers [10]. On the other hand, another associated issue is the efficient optical amplification when longer reach is targeted. Optical amplification solutions operating in the O-, C-, and L-band are currently commercially available. In addition, rare-earth-doped fibre amplifiers, such as the Bismuth-doped fibre amplifier (BDFEA) [22], [23] and the Thulium-doped fibre amplifier (TDFEA) [24], [25], have also demonstrated their effectiveness of high-gain optical amplification over O-, E-, and S-bands. These amplification techniques can be combined together with the NANF to realise ultra-wideband long-distance transmission.

IV. CONCLUSION

We have reported the first ultra-wide bandwidth, low loss NANF operating in the *first* antiresonant passband. The fiber has a very flat 700 nm 3-dB bandwidth that includes the O-, S-, C- and L-bands, and the lowest loss (6.6 dB/km) ever reported in an ultra-wide bandwidth ARF operating in the *first* passband with relatively thin membrane struts. The excellent modal purity of the fiber allows penalty-free transmission of 100-Gbit/s PAM4 signals from the O to L-band over ~1 km of fiber. Although already potentially interesting for some short-reach low-latency applications, the current loss level, limited by asymmetries and the large inter-tube gaps, can be significantly reduced in future iterations. The predicted sub-dB/km ultra-wide bandwidth, which appears realistically achievable, could make NANFs a very promising solution for future high-speed, low-latency intra/inter datacenter, 5G and short-reach optical communications.

ACKNOWLEDGMENT

The authors would like to thank Simon Bawn, Lumenicity Ltd., for help with splicing. All data supporting this study are

openly available from the University of Southampton repository at: <https://doi.org/10.5258/SOTON/D1083>.

REFERENCES

- [1] F. Poletti *et al.*, "Towards high-capacity fibre-optic communications at the speed of light in vacuum," *Nature Photon.*, vol. 7, no. 4, pp. 279–284, 2013.
- [2] B. J. Mangan *et al.*, "Low loss (1.7 dB/km) hollow core photonic bandgap fiber," in *Proc. Opt. Fiber Commun. Conf.*, 2004, Paper PDP5A.2.F.
- [3] C. Peucheret, B. Zsigri, T. P. Hansen, and P. Jeppesen, "10 Gbit/s transmission over air-guiding photonic bandgap fibre at 1550 nm," *Electron. Lett.*, vol. 41, no. 1, pp. 27–29, 2005.
- [4] N. V. Wheeler *et al.*, "Wide-bandwidth, low-loss, 19-cell hollow core photonic band gap fiber and its potential for low latency data transmission," in *Proc. OFC/NFOEC*, 2012, Paper PDP5A.2.F.
- [5] V. A. J. M. Sleiffer *et al.*, "High capacity mode-division multiplexed optical transmission in a novel 37-cell hollow-core photonic bandgap fiber," *J. Lightw. Technol.*, vol. 32, no. 4, pp. 854–863, Feb. 2014.
- [6] A. N. Kolyadin, A. F. Kosolapov, A. D. Pryamikov, A. S. Biriukov, V. G. Plotnichenko, and E. M. Dianov, "Light transmission in negative curvature hollow core fiber in extremely high material loss region," *Opt. Express*, vol. 21, no. 8, pp. 9514–9519, 2013.
- [7] B. Debord *et al.*, "Ultralow transmission loss in inhibited-coupling guiding hollow fibers," *Optica*, vol. 4, no. 2, pp. 209–217, 2017.
- [8] J. R. Hayes *et al.*, "Antiresonant hollow core fiber with octave spanning bandwidth for short haul data communications," in *Proc. Opt. Fiber Commun. Conf. Exhib.*, 2016, Paper PDP TH5A.3.
- [9] S. Gao *et al.*, "Hollow-core conjoined-tube negative-curvature fibre with ultralow loss," *Nature Commun.*, vol. 9, no. 1, 2018, Art. no. 2828.
- [10] F. Poletti, "Nested antiresonant nodeless hollow core fiber," *Opt. Express*, vol. 22, no. 20, pp. 23807–23828, 2014.
- [11] T. D. Bradley *et al.*, "Record low-loss 1.3dB/km data transmitting antiresonant hollow core fibre," in *Proc. Eur. Conf. Opt. Commun.*, 2018, pp. 1–3.
- [12] G. T. Jasion *et al.*, "Virtual draw of tubular hollow-core fibers," in *Proc. Frontiers Optics/Laser Sci.*, 2018, Paper FW6B.3.
- [13] H. Sakr *et al.*, "Ultrawide bandwidth hollow core fiber for interband short reach data transmission," in *Proc. Opt. Fiber Commun. Conf.*, 2019, Paper PDP Th4A.1.
- [14] J. R. Hayes, F. Poletti, M. S. Abokhamis, N. V. Wheeler, N. K. Baddela, and D. J. Richardson, "Anti-resonant hexagram hollow core fibers," *Opt. Express*, vol. 23, no. 2, pp. 1289–1299, 2015.
- [15] E. N. Fokoua, Y. Chen, D. J. Richardson, and F. Poletti, "Microbending effects in hollow-core photonic bandgap fibers," in *Proc. 42nd Eur. Conf. Opt. Commun.*, 2016, pp. 327–329.
- [16] L. Vincetti and V. Setti, "Waveguiding mechanism in tube lattice fibers," *Opt. Express*, vol. 18, no. 22, pp. 23133–23146, 2010.
- [17] H. Sakr *et al.*, "Record low loss hollow core fiber for the 1 μ m region," in *Proc. Conf. Lasers Electro-Optics/Europe Eur. Quantum Electron. Conf.*, 2019, Paper CE_5_5.
- [18] Y. Hong *et al.*, "Beyond 100-Gb/s/λ direct-detection transmission over the S+C+L-bands in an ultra-wide bandwidth hollow core fibre," in *Proc. ECOC*, 2019, Paper Th.2.E.5.
- [19] Z. Liu *et al.*, "Nonlinearity-free coherent transmission in hollow-core antiresonant fiber," *J. Lightw. Technol.*, vol. 37, no. 3, pp. 909–916, Feb. 2019.
- [20] T. K. Chan and W. I. Way, "112 Gb/s PAM4 transmission over 40 km SSMF using 1.3 μ m gain-clamped semiconductor optical amplifier," in *Proc. Opt. Fiber Commun. Conf. Exhib.*, 2015, Paper Th3A.4.
- [21] Z. Wang and A. Ghiasi, "400GE lane configurations v.s. FEC options," in *Proc. IEEE 802.3 Plenary Meeting*, Jul. 2013. [Online]. Available: http://www.ieee802.org/3/400GSG/public/13_07/wang_400_01_0713.pdf
- [22] E. M. Dianov, "Bismuth-doped optical fibers: A challenging active medium for near-IR lasers and optical amplifiers," *Light Sci. Appl.*, vol. 1, 2012, pp. 1–7, Art. no. e12.
- [23] N. K. Thipparapu, Y. Wang, A. A. Umnikov, P. Barua, D. J. Richardson, and J. K. Sahu, "40 dB gain all fiber bismuth-doped amplifier operating in the O-band," *Opt. Lett.*, vol. 44, no. 9, pp. 2248–2251, 2019.
- [24] B. N. Samson *et al.*, "Thulium-doped silicate fiber amplifier at 1460–1520 nm," in *Proc. Opt. Amplifiers Appl.*, 2001, pp. 247–248.
- [25] S. Aozasa and M. Yamada, "E-band thulium doped fibre amplifier," *Electron. Lett.*, vol. 55, no. 6, pp. 333–334, 2019.